Behaviours of circular CFDST with stainless steel external tube: Slender columns and beams

Hui Zhao [a], Rui Wang [a,*], Dennis Lam [b], Chuan-Chuan Hou [c], Rong Zhang [d]

a *School of Civil Engineering, Taiyuan University of Technology, Taiyuan 030024, China*

b *Faculty of Engineering and Informatics, University of Bradford, Bradford BD7 1DP, UK*

c *School of Transportation Science and Engineering, Beihang University, Beijing 100191, China*

d *Department of Mechanical Engineering and Automation, Harbin Institute of Technology (Shenzhen), ShenZhen 518055, China*

Abstract

This paper presents the experimental and numerical studies on the performance of circular concrete filled double steel tubular (CFDST) slender columns and beams with external stainless steel tube. Twenty-four specimens, including 18 slender columns and 6 beams were tested to obtain the failure patterns, load versus deflection relationships and longitudinal strain developments in the stainless steel tube. Finite element (FE) models were established and verified by test results. The validated FE models were then employed to investigate the influences of key parameters, including hollow ratio, eccentric ratio and material strength, on the load-bearing capacity. The load distribution among the components and contact stress between sandwiched concrete and steel tubes were also analyzed. Finally, the design methods for CFDST and hollow CFST members with external carbon steel tube respectively suggested by Han et al. (2018) and Chinese GB 50936-2014 (2014) were employed to evaluate their applicability for the circular CFDST slender columns and beams with outer stainless steel tube.

Keywords: Concrete filled double steel tubular; Stainless steel tube; Compression; Hollow ratio; FE modelling.

1. Introduction

Concrete filled double skin steel tube (CFDST) member as presented in Fig. 1 is produced with two concentric steel tubes and concrete filled between two tubes [1-3]. In the past twenty years, large numbers of researches have been conducted on the behaviours of such members under different load conditions, including the static [4-9], dynamic [10-12] and fire [13] loadings. Available research results have indicated that the CFDST members present greater flexural capacity and better seismic resistance when compared to the concrete filled steel tube (CFST) members. In addition, owing to the internal steel tube being thermally protected by the concrete, such members also exhibit good fire resistance. Considering above several advantages, this type of composite member has been increasingly utilized in bridge piers, transmission towers and electrical grid structures, etc. [3, 14, 15]

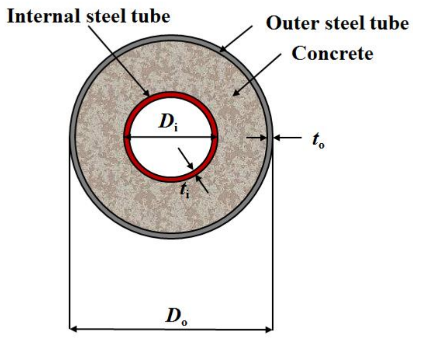

Fig.1. Cross-section of CFDST member.

Recently, stainless steel outer tube has been employed in the construction application, which is due to its better corrosion, fire and impact resistances, and maintenance when compared to the carbon steel [16-18]. In addition, stainless steel presents strong strain-hardening behaviour without a definite yield strength and excellent ductility, i.e., the elongation of stainless steel after fracture can reach about 50% [18]. However, the price of stainless steel inhibits its wide application in construction. To economically and efficiently use of this material, a CFDST section with a stainless steel outer tube was developed [19]. Han et al. [19] conducted tests on 80 CFDST stub columns with stainless steel external tube under axial loading, and found that their compression behaviours are similar to those of double carbon-skin composite columns. The ultimate load-bearing capacities of such stub columns were analyzed using finite element methods by Hassanein et al. [20] and Wang et al. [21]. In 2019, Wang et al. [22] experimentally and numerically investigated the compressive behaviours of CFDST short columns having stainless steel external tube and high strength steel internal tube. The results have indicated that the design models for CFST members generally provide conservative predictions of CFDST stub columns. However, limited researches have been conducted on the performance of CFDST slender columns and beams having stainless steel external tube. The only available study on such slender columns was conducted by Hassanein and Kharoob [23] using the FE method. According to numerical results, the authors concluded that the design load-carrying capacities of CFST slender columns given by AISC specification [24] and EC 4 [25] overestimate the compressive capacities of CFDST slender columns with the stainless steel jacket. Until now, no experimental researches on such slender columns and beams have been undertaken.

Consequently, this work aims to investigate the performance of the CFDST slender columns and beams with external stainless steel tube. For this purpose, a total of 24 specimens were tested. The finite element (FE) models were established to validate the experimental results and employed to perform parametric studies to expand the ranges of hollow ratio, load eccentricity ratio and material strength. The load distribution among the components and contact stress between sandwiched concrete and steel tubes were also investigated using the FE models. Finally, all the FE and experimental results were compared with the load-bearing capacity predictions for the composite members with carbon steel external tube suggested by Han et al. [3] and Chinese GB 50936 [26].

2. Test program

2.1. Specimen preparations

Twenty-four circular CFDST specimens with internal carbon and external stainless steel tubes were examined, including 18 slender columns and 6 beams. Details about column and beam specimens are presented in Table 1 and Table 2, respectively. The key parameters are hollow ratio, $\chi=D_i/(D_o-2t_o)$ (in which D_i and D_o respectively represent the outer diameter of internal carbon and outer stainless steel tube and t_o is the thickness of the outer tube), slenderness ratio λ and load eccentricity e. The slenderness ratio λ greater than 22 is applied to define the CFDST slender column, as suggested by Hassanein and Kharoob [23]. The identification system of all specimens (Table 1 and Table 2) is defined as follows:

- The first characters "C" and "B" represent the column and beam specimen, respectively.
- The first numbers "1", "2" and "3" stand for the specimen lengths corresponding to 800 mm, 1300 mm and 1800 mm, respectively.
- The following numbers "0.44", "0.69" and "0.81" account for the hollow ratio.
- The next numbers "4" and "14" denote the eccentricity of applied load on the column.
- The last letters "a" and "b" represent the first and second specimen in one group, respectively.

Table 1 Details of column specimens.

No.	Specimen label	External stainless tube	Inner carbon tube	χ	L	e	λ
		$D_o \times t_o$(mm)	$D_i \times t_i$(mm)		(mm)	(mm)	
1	C1-0.44-4-a	114×1.88	48×2.52	0.44	800	4	23
2	C1-0.44-4-b	114×1.88	48×2.52	0.44	800	4	23
3	C1-0.69-14-a	114×1.88	76×2.01	0.69	800	14	22
4	C1-0.69-14-b	114×1.88	76×2.01	0.69	800	14	22
5	C2-0.44-4-a	114×1.88	48×2.52	0.44	1300	4	38
6	C2-0.44-4-b	114×1.88	48×2.52	0.44	1300	4	38
7	C2-0.69-14-a	114×1.88	76×2.01	0.69	1300	14	35
8	C2-0.69-14-b	114×1.88	76×2.01	0.69	1300	14	35
9	C3-0.44-4-a	114×1.88	48×2.52	0.44	1800	4	53
10	C3-0.44-4-b	114×1.88	48×2.52	0.44	1800	4	53
11	C3-0.69-14-a	114×1.88	76×2.01	0.69	1800	14	49
12	C3-0.69-14-b	114×1.88	76×2.01	0.69	1800	14	49

Table 2 Details of beam specimens.

No.	Specimen label	External stainless tube	Inner carbon tube	χ	L	l/D_o
		$D_o \times t_o$(mm)	$D_i \times t_i$(mm)		(mm)	
1	B3-0.44-a	114×1.88	48×2.52	0.44	1800	5
2	B3-0.44-b	114×1.88	48×2.52	0.44	1800	5
3	B3-0.69-a	114×1.88	76×2.01	0.69	1800	5
4	B3-0.69-b	114×1.88	76×2.01	0.69	1800	5
5	B3-0.81-a	114×1.88	89×2.01	0.81	1800	5
6	B3-0.81-b	114×1.88	89×2.01	0.81	1800	5

Note: t_i is the internal tube thickness, L is the specimen length, l is the shear span.

The specimens were made in the following procedures: both the outer stainless and inner carbon steel tubes were first cut from the long tubes, next, a steel plate was welded to one end of both inner and outer tubes at the designed position. Self-consolidating concrete was then poured into the gap between the inner and outer tubes. For column specimens, the concrete was filled slightly higher than both steel tubes to avoid the gap between the concrete and steel plate. Before testing, the column specimen was surface treated and sealed by the other end plate. For beam specimens, the steel plate was removed and the two ends were uncapped.

2.2. Material properties

Material properties of carbon and stainless steels were determined from the tensile test in accordance with ISO 6892-1 [27]. All tensile steel coupons were extracted from the steel tubes. Owing to the rounded stress-strain response of stainless steel, the 0.2% proof stress ($\sigma_{0.2}$) is used to specify the yield stress [17, 18]. Table 3 presents the average yield stress σ_y, ultimate stress σ_u, modulus of elasticity E_s and elongation δ for all steels. The cube (150 mm×150 mm×150 mm) compressive strength ($f_{cu,28d}$ and $f_{cu,test}$) and prism (150 mm×150 mm×300 mm) elastic modulus ($E_{c,test}$) are given in Table 4.

Table 3 Material properties of carbon and stainless steels.

	σ_y /MPa	σ_u/MPa	E_s/MPa	δ
Carbon steel (2.01 mm)	275	351	2.08×10^5	0.22
Carbon steel (2.52 mm)	276	384	2.05×10^5	0.25
Stainless steel (1.88 mm)	322	703	1.91×10^5	0.46

Table 4 Compressive properties of concrete.

$f_{cu,28d}$/MPa	$f_{cu,test}$/MPa	$E_{c,test}$/MPa

55.3	60.2	3.1×10^{4}

2.3. Test apparatus and procedures

The column specimens were tested using a hydraulic compression machine with a loading capacity of 5000 kN. Figs. 2 and 3 present the loading setup and instrument arrangement for slender columns and beams, respectively. For the slender column under compression, the high strength steel plate with 6 mm deep groove and the knife edge were employed at both ends of specimens to achieve the pinned-end conditions and different loading eccentricities (Fig. 2). The compression load was applied through the knife edge . Three displacement transducers were respectively employed to monitor the lateral deflections corresponding to 1/4*L*, 1/2*L* and 3/4*L*. Strain gauges were used to monitor the longitudinal strains of stainless steel tube at the 1/2-height of the column, as presented in Fig. 2(b).

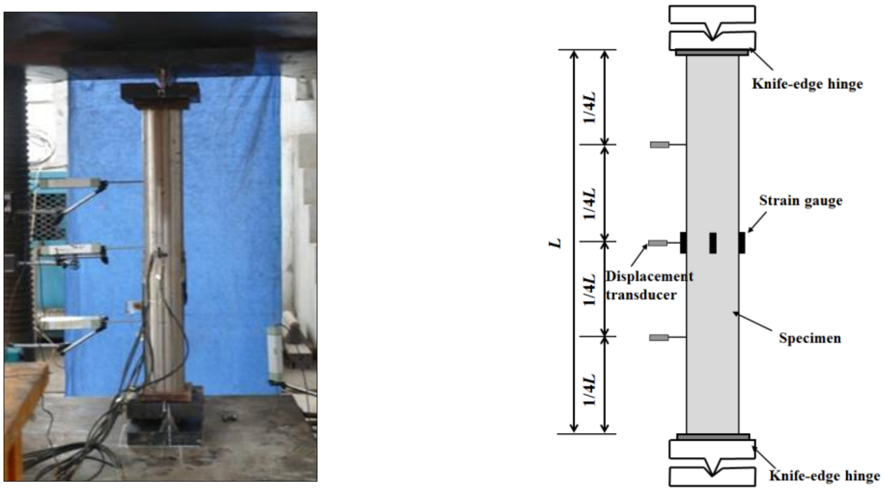

(a) Test scene (b) Schematic view

Fig.2. Loading setup and instrument arrangement for slender column specimen.

For the prue bending test, a four-points testing rig was employed to apply the moment as shown in Fig. 3. Han et al. [28] found that the shear span-to-depth ratio varying between 1.25 and 6 had an insignificant effect on the moment-curvature curves of the CFST beams. Therefore, the shear span-to-depth ratio of 5 and two-point loads were used in the test. The in-plane deflections were monitored by three displacement transducers along the beam. Strain gauges were employed for monitoring the strain developments at the 1/2-span section.

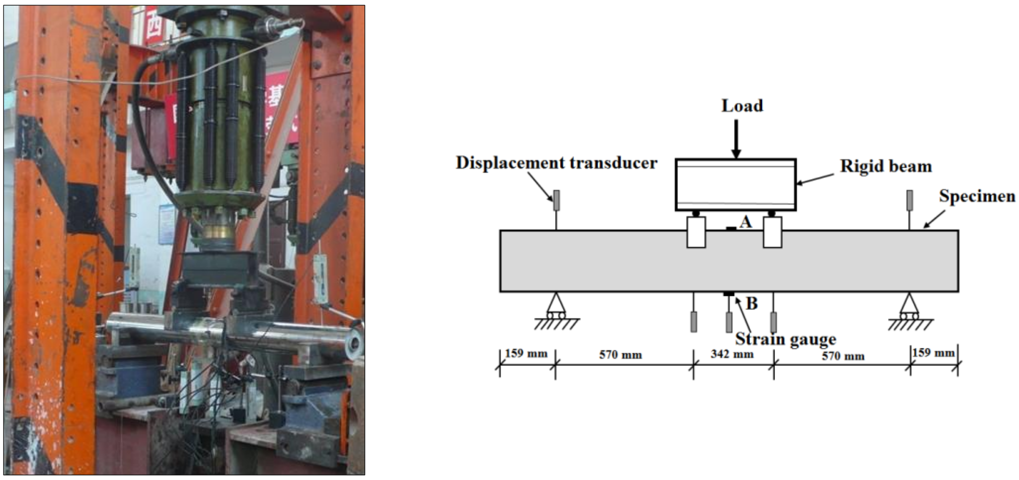

(a) Test scene (b) Schematic view

Fig.3. Loading setup and instrument arrangement for beam specimen.

The load was force-controlled at a rate of 2 kN/s up to approximately 85% of the estimated load-bearing resistance, and then displacement control was adopted to capture the post-peak curve of the specimen. The loading interval was less than 10% of the load-bearing capacity estimated by FE model. Each load interval was sustained for around 2 min to record the data and observe the phenomenon.

2.4. Test results and discussions

The failure patterns of all specimens are presented in Fig. 4. For the slender columns, a typical global buckling with large lateral deflection was observed (Fig. 4(a)). The local buckling at the 1/2-height section was unobvious due to the presence of sandwiched concrete, except for specimen C1-0.69-14. Similar failure patterns were also observed on the conventional CFST and CFDST columns with external carbon steel tube [5, 29-31]. There was no significant difference in the failure pattern between specimens with hollow ratios of 0.44 and 0.69.

The typical failure pattern of the beam specimens is presented in Fig. 4(b). It is noted that an outward folding failure formed in the CFDST beams with external stainless steel tube under bending, all specimens were failed in a ductile manner. This is similar to that found in the CFST beam [28, 32]. An unobvious difference was observed among specimens with varying hollow ratio. Unlike the hollow tube, the specimens presented an insignificant outward local buckling at the compression side. The external steel tube of beam specimens was removed after bending, as presented in Fig. 4(b). It can be found that the sandwiched concrete maintained intact, and tensile cracks mainly occurred at the bottom of the 1/2-span section.

(a) Slender column specimens

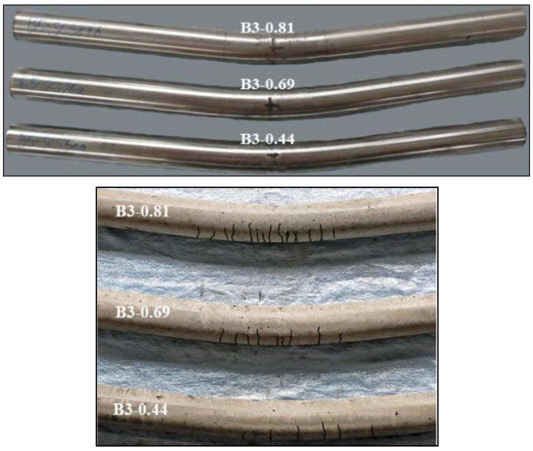

(b) Beam specimens

Fig.4. Failure patterns of specimens.

The axial load vs. deflection and longitudinal strain at the mid-height of column specimens are presented in Figs. 5 and 6. Generally, the axial load vs. mid-height deflection curves exhibited three phases: elastic , elasto-plastic with decreasing stiffness, and post failure (Fig. 5). The lateral deflection at the mid-height was not obvious before reaching the maximum load, and it increased rapidly during the post-peak phase. As expected, the load-carrying capacity of the column specimens decreased with the increase of slenderness ratio. As presented in Fig. 6, the compression and tension zones on the mid-height section exhibited simultaneously at the beginning of eccentric loading stage, mainly due to the obvious second-order effect.

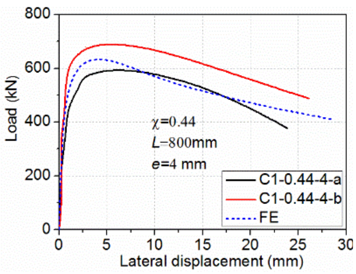

(a) C1-0.44-4

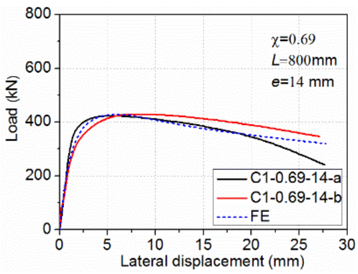

(b) C1-0.69-14

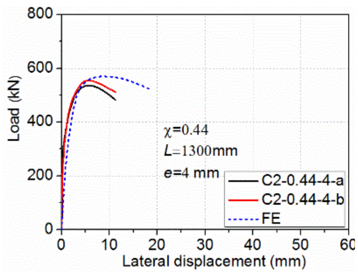

(c) C2-0.44-4

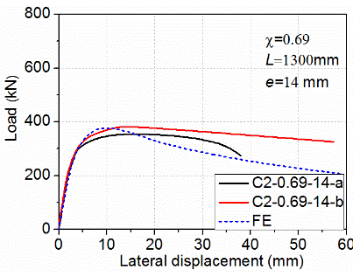

(d) C2-0.69-14

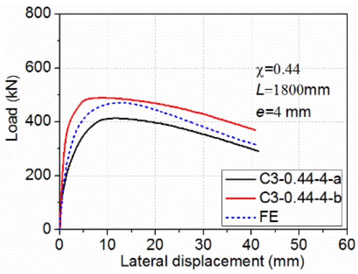

(e) C3-0.44-4

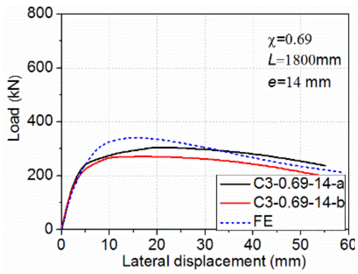

(f) C3-0.69-14

Fig.5. Axial load vs. mid-height deflection (slender column).

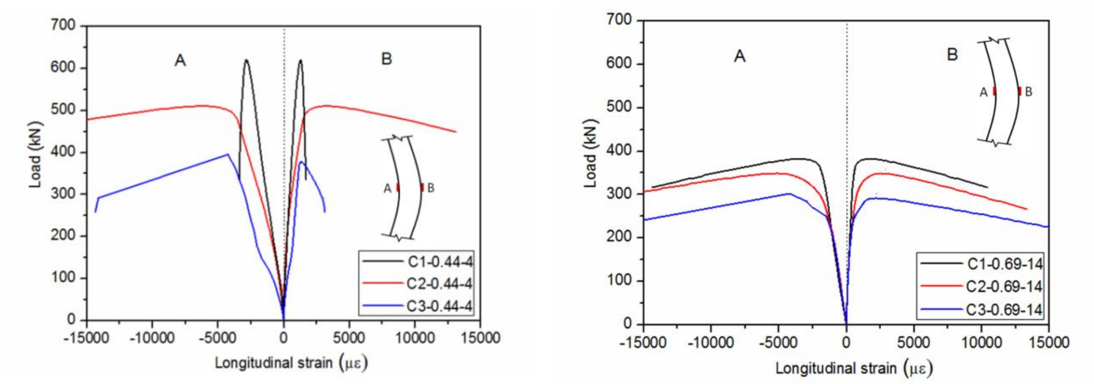

(a) (b)

Fig.6. Axial load vs. longitudinal strain at the mid-height (slender column).

Figs. 7 and 8 present the moment vs. deflection and longitudinal strain at the mid-span of beam specimens. It can also be seen from these curves that the CFDST beams with external stainless steel tube exhibited good ductility. Under pure bending, the response of all specimens showed elastic and plastic deformation phases until the ultimate moment resistance was reached. As suggested by Han [32], considering the practice condition, the moment capacity of composite beam is taken as the moment at the maximum fiber tensile strain of 10000 με. The moment capacities of beam specimens with hollow ratios of 0.44, 0.69 and 0.81 were 13.3, 15.0 and 14.0 kN·m, respectively. Specimens with hollow ratios of 0.69 and 0.81 presented relatively high values when compared to that having hollow ratio of 0.44, which is mainly owing to the larger flexural resistance by increasing the diameter of internal steel tube.

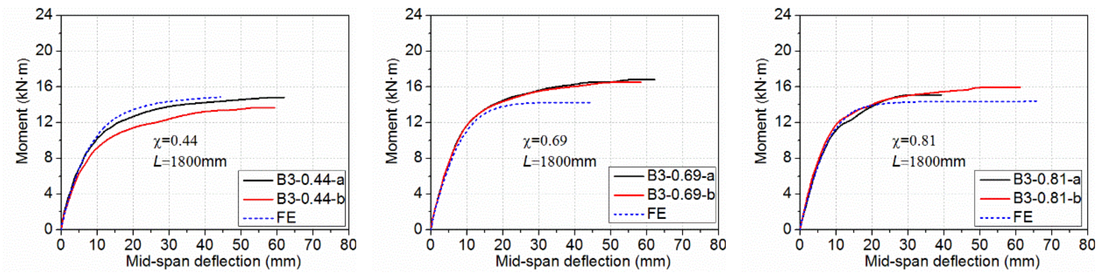

(a) B3-0.44 (b) B3-0.69 (c) B3-0.81

Fig.7. Moment vs. mid-span deflection (beam).

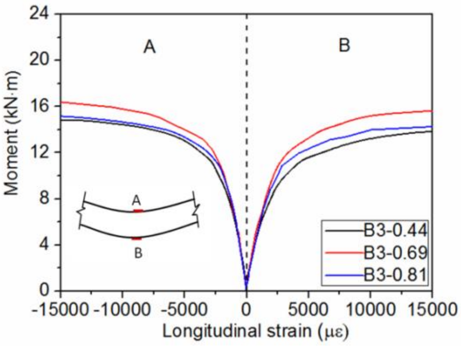

Fig.8. Moment vs. longitudinal strain at the mid-span (beam).

3. Finite element (FE) analysis

3.1. FE modeling

In this section, to further study the structural behaviours of the CFDST members with external stainless steel tube under compression and bending, the program ABAQUS was employed to develop the FE model. The material models and stainless/carbon steel-concrete interface were presented in detail. These FE models were verified against the test results.

Typical FE models for the slender columns and beams are presented in Fig. 9, where the boundary condition, loading and mesh size are shown. The reference points in the models were employed to apply the boundary restrain and loading. C3D8R (8-noded solid element) and S4R (4-noded shell element) were respectively utilized for the sandwiched concrete and the carbon/stainless steel tube. It is well documented that the slender member is affected by the initial global imperfection. There were two phases to introduce the imperfection. Firstly, the buckling analysis was conducted to obtain the first buckling mode. In the second phase, the first eigenmode multiplied by a factor of 0.001L (L is the specimen length) was introduced into the loading model [31, 33].

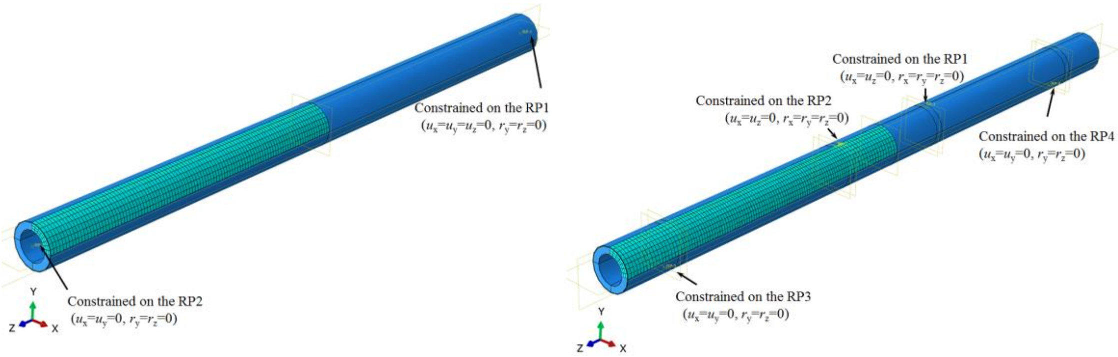

(a) Slender column (b) Beam

Fig.9.View of FE models for slender column and beam in ABAQUS.

In this work, a 5-stage stress-strain model suggested by Han et al. [34] was employed to model the carbon steel. Stainless steel presents a rounded stress-strain behaviour and pronounced strain hardening. A 2-stage stress-strain model suggested by Rasmussen [35] was used to simulate the material stress-strain response of stainless steel, as presented in Eq. (1).

$$\varepsilon=\begin{cases}\frac{\sigma}{E_0}+0.002\left(\frac{\sigma}{\sigma_{0.2}}\right)^n & \sigma\leq\sigma_{0.2}\\ \frac{\sigma-\sigma_{0.2}}{E_{0.2}}+\varepsilon_u\left(\frac{\sigma-\sigma_{0.2}}{\sigma_u-\sigma_{0.2}}\right)^m+\varepsilon_{0.2} & \sigma>\sigma_{0.2}\end{cases} \tag{1a}$$

$$n=\frac{\ln 20}{\ln\left(\sigma_{0.2}/\sigma_{0.01}\right)} \tag{1b}$$

$$E_{0.2}=\frac{E_0}{1+0.002n/e} \tag{1c}$$

$$e=\frac{\sigma_{0.2}}{E_0} \tag{1d}$$

$$m=1+3.5\frac{\sigma_{0.2}}{\sigma_u} \tag{1e}$$

$$\varepsilon_{0.2}=\frac{\sigma_{0.2}}{E_0}+0.002 \tag{1f}$$

in which σ= stress, ε= strain, E_0= initial modulus of elasticity of stainless steel, $\sigma_{0.2}$= stress corresponding to 0.2% plastic strain, $E_{0.2}$= tangent modulus at the $\sigma_{0.2}$, σ_u= ultimate stress, ε_u= ultimate strain, n and m are strain hardening coefficients.

Tao et al. [36] found that the confinement effect provided by the stainless steel tube to the core concrete was similar to that by the carbon steel tube. Therefore, the concrete compressive model used in the CFDST member with external carbon steel tube [21] was adopted in the simulation of the sandwiched concrete, as given in Eq. (2).

$$y=\begin{cases}2x-x^2 & x\leq 1\\ \frac{x}{\beta_0(x-1)^\eta+x} & x>1\end{cases} \tag{2a}$$

$$x=\varepsilon/\varepsilon_0 \tag{2b}$$

$$y=\sigma/f_c' \tag{2c}$$

$$\varepsilon_0=\varepsilon_c+800\cdot\xi^{0.2}\cdot 10^{-6} \tag{2d}$$

$$\varepsilon_c=(1300+12.5\cdot f_c')\cdot 10^{-6} \tag{2e}$$

$$\beta_0=0.5\left(2.36\times10^{-5}\right)^{\left[0.25+(\xi-0.5)^7\right]}\left(f_c'\right)^{0.5}\geq 0.12 \tag{2f}$$

$$\xi = \frac{A_{so} \cdot f_{yo}}{A_{c,\ nominal} \cdot f_{ck}} \tag{2g}$$

in which f_c'= concrete cylinder strength, f_{ck}= characteristic concrete strength (f_{ck}=0.67 f_{cu}, where f_{cu}=cube strength of concrete), f_{yo}= yield stress of outer steel tube, A_{so}= cross-section area of the outer tube, $A_{c,\ nominal}$= the nominal cross-section area of the concrete ($A_{c,\ nominal}$= π $(D_o\text{-}2t_o)^2/4$); η= 2 for circular section.

The "concrete damaged plasticity model" in ABAQUS material was employed to describe the inelasticity of the sandwiched concrete. The linear stress-strain model suggested in Refs [37, 38] was adopted in the modeling of the sandwiched concrete in tension, as expressed in Eq. (3).

$$\sigma = \begin{cases} E_c\,\varepsilon & \varepsilon \le \varepsilon_{cr} \\ f_t'\left(\dfrac{\varepsilon - \varepsilon_{tu}}{\varepsilon_{cr} - \varepsilon_{tu}}\right) & \varepsilon_{cr} < \varepsilon \le \varepsilon_{tu} \\ 0 & \varepsilon > \varepsilon_{tu} \end{cases} \tag{3}$$

in which E_c= modulus of elasticity of concrete (E_c =4700$\sqrt{f_c'}$), f_t'=0.1 f_c', ε_{cr}= f_t'/ E_c , ε_{tu}=15ε_{cr}.

The interaction behaviour between the sandwiched concrete and steel tube was defined by the Coulomb's friction model along the tangential direction and hard-contact model along the normal direction. The sandwiched concrete was chosen as the master surface, where the surface of external/internal steel tube was defined as the slave. The friction coefficient between the concrete and the stainless steel tube was adopted as 0.25 [23], while the value of 0.6 was defined between the concrete and carbon steel tube. The appropriate mesh density was determined by the mesh convergence studies. A mesh size of D_o/20 over the cross-section was chosen for the model, where D_o is the the outer diameter of external steel tube.

3.2. Verification of the FE model

In order to verify the FE models, the predicted curves of load vs. mid-span deflection are compared with those obtained experimentally, as presented in Figs. 5 and 7. The features of the complete test curve include the stiffness, ultimate strength and load-deflection development of the specimen. Fig. 10 shows the comparisons between experimental and numerical ultimate loads. The average ratio of the FE results to experimental results is 0.97, with a standard deviation of 0.01. Generally, the FE models could replicate the load-deflection curves and failure patterns for the tested CFDST slender columns and beams having stainless steel external tube. In some cases, the predicted curves are not the same with the experimental results, mainly owing to the experimental error and the material property deviations between the simulation and test.

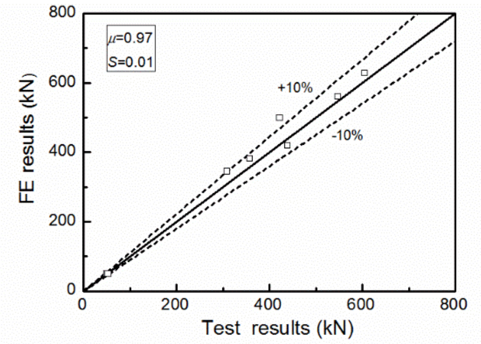

Fig.10. Comparison between FE and test results.

4. Parametric investigations and design methods

4.1. Parametric investigations

After validating the FE methodmodels, extensive parametric investigations were conducted to extend the ranges of hollow ratio, load eccentricity ratio, yield stress of external and internal steel tubes and concrete strength. The parameters investigated are presented in Tables 5 and 6. The yield strength of stainless steel is taken as the stress at 0.2% plastic strain. In order to investigate the hollow ratio (χ) on the behaviour of slender columns and beams, the only dimension variation was made in the internal tube diameter (D_i).

Table 5 Parametric investigations for slender columns.

Case	Outer tube		Inner tube		χ	L	λ	e/r_o	f_{yo}	f_{yi}	f_{cu}
	D_o(mm)	t_o(mm)	D_i(mm)	t_i(mm)		(mm)			(MPa)	(MPa)	(MPa)
Column	400	10	114	4	0.3	4500	43.0	0, 0.2, 0.4	230, 380	235, 390	30, 50
	400	10	190	4	0.5	4500	41.0	0, 0.2, 0.4	230, 380	235, 390	30, 50
	400	10	266	4	0.7	4500	37.0	0, 0.2, 0.4	230, 380	235, 390	30, 50
	600	10	174	4	0.3	4500	29.0	0, 0.2, 0.4	230, 380	235, 390	30, 50
	600	10	290	4	0.5	4500	27.0	0, 0.2, 0.4	230, 380	235, 390	30, 50

	600	10	406	4	0.7	4500	25.0	0, 0.4	0.2,	230, 380	235, 390	30, 50

Table 6 Parametric investigations for beams.

Case	Outer tube		Inner tube		χ	L	l/D_o	f_{yo}	f_{yi}	f_{cu}
	D_o(mm)	t_o(mm)	D_i(mm)	t_i(mm)		(mm)		(MPa)	(MPa)	(MPa)
Beam	400	10	114	4	0.3	4500	5	230, 380	235, 390	30, 50
	400	10	190	4	0.5	4500	5	230, 380	235, 390	30, 50
	400	10	266	4	0.7	4500	5	230, 380	235, 390	30, 50
	600	10	174	4	0.3	4500	5	230, 380	235, 390	30, 50
	600	10	290	4	0.5	4500	5	230, 380	235, 390	30, 50
	600	10	406	4	0.7	4500	5	230, 380	235, 390	30, 50

Note: L is the column and beam length; f_{yo} and f_{yi} are respectively the yield strength of outer and inner steel tube; f_{cu} is the cubic compressive strength of sandwiched concrete; e is the load eccentricity; r_o is the outer radius of external steel tube; l is the shear span.

4.1.1 Influences of key parameters

Fig. 11 presents the effects of key parameters on the load-carrying capacities of slender columns. As shown in Fig. 11(a), for columns with a diameter of 600 mm, increasing hollow ratio from 0.3 to 0.5 hardly affects the ultimate strengths. Columns having hollow ratio of 0.7 show the lowest load-carrying capacities. For columns with a diameter of 400 mm, the highest ultimate strength was found at the hollow ratio of 0.5. Above changes are mainly related to the variations in the cross-sectional area of concrete and the flexural rigidity of the inner steel tube. The reduction in the area of concrete induces a decrease in the ultimate strength, whereas the increasing flexural rigidity caused by moving the inner tube farther from the centroid increases the column strength. In Fig. 11, the load-carrying capacities decrease with the increase in the load eccentricity ratio, and increase with the increasing yield stress of outer steel tube and concrete strength. It can be seen that the strength of internal steel tube has a minor effect on the ultimate load of slender columns. This is mainly because that the flexural resistance is marginally affected by the variation in the strength of inner steel tube which is located near the neutral axis.

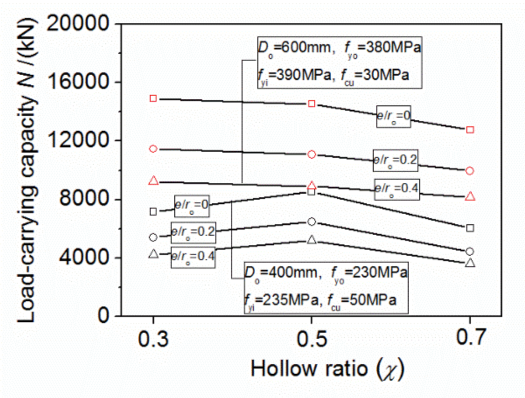

(a) Hollow ratio (χ)

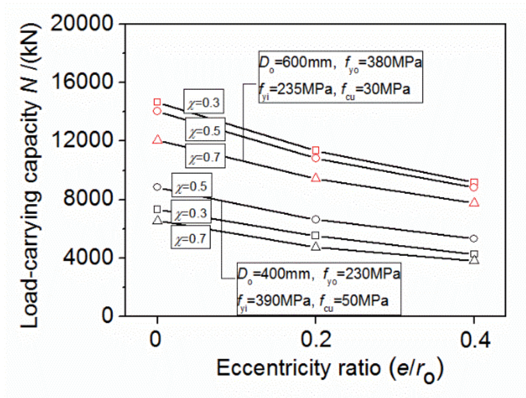

(b) Load eccentricity ratio (e/r_o)

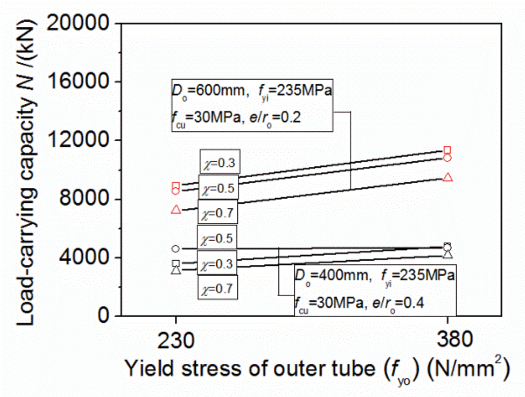

(c) Yield stress of external steel tube (f_{yo})

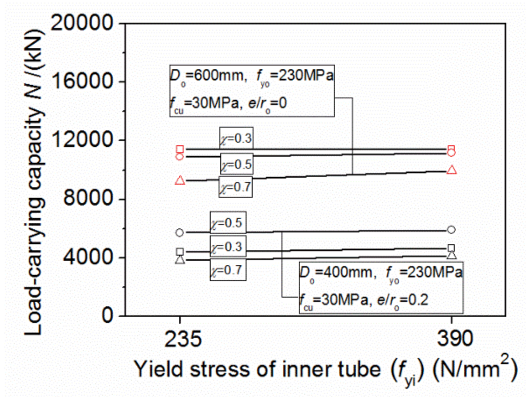

(d) Yield stress of internal steel tube (f_{yi})

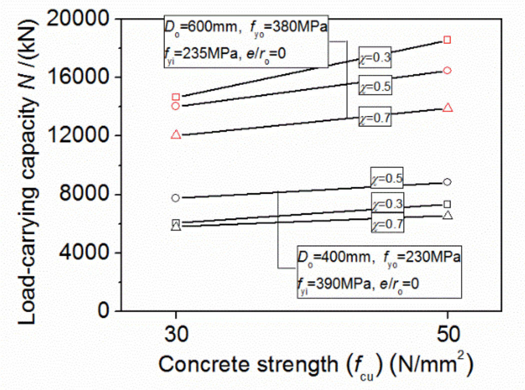

(e) Concrete strength (f_{cu})

Fig.11. Effect of parameters on the load-carrying capacities of slender columns.

The effects of these parameters on the moment capacities of beams are presented in Fig. 12. Similar to the load-carrying capacities of slender columns, the bending capacities of beams also increase significantly with increasing yield stress of external steel tube. As with the hollow ratio increases from 0.3 to 0.7, the change in the bending capacity is not obvious. The strengths of internal steel tube and concrete have a marginal effect on the flexural resistance. Based on the analysis of Figs. 11 and 12, it is structural efficiency to employ the high-strength outer steel tube and hollow ratio of 0.5 in CFDST member under combined compression and bending.

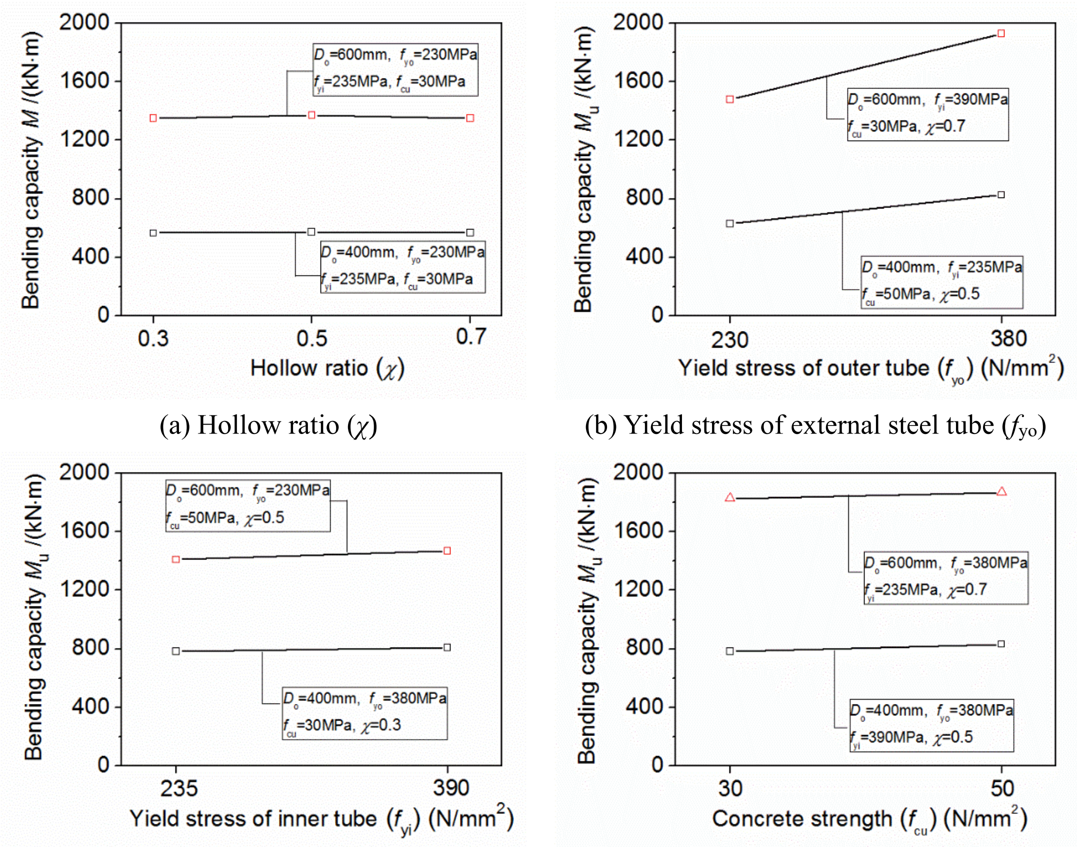

(a) Hollow ratio (χ) (b) Yield stress of external steel tube (f_{yo})

(c) Yield stress of internal steel tube (f_{yi}) (d) Concrete strength (f_{cu})

Fig.12. Effect of parameters on the moment capacities of beams.

4.1.2 Load distribution and confinement effect

The load distributions among the outer and inner steel tubes as well as sandwiched concrete were analyzed, as shown in Fig. 13. For the slender column, all the steel tubes and concrete components carry the compression load during the whole loading phase, and sandwiched concrete contributes a large portion of the axial resistance (Fig. 13(a)). At the ultimate strength, the axial-load contribution percentages of sandwiched concrete, outer and inner steel tubes are 58.1%, 30.9% and 11.0%, respectively. Due to the confinement from the steel tube, the load carried by the whole CFDST member declines, while the load of the sandwiched concrete remains increasing. For the beam in Fig. 13(b), the majority of bending moment is carried by the outer steel tube because of the large distance from the neutral axis.

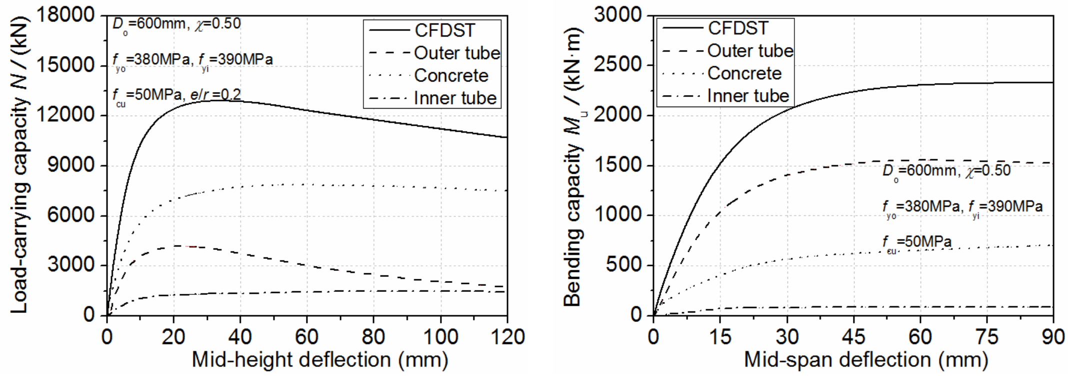

(a) Slender columns (b) Beams

Fig.13. Load distributions in slender columns and beams.

Fig. 14 presents the contact stress between steel tube and sandwiched concrete at the mid-span section of slender columns and beams. For CFDST slender column in Fig. 14(a), the contact stress does not exist in the initial phase of loading because the Poisson's ratio of sandwiched concrete is smaller compared with that of the steel tube. With the increasing load, the contact stress between the outer tube and concrete begins to develop, which is mainly due to enlarged lateral expansion of the concrete exceeds that of the steel tube during the elastic-plastic phase. It clearly shows that the confinement provided by the outer tube is greater than that by the inner tube in Fig. 14(a). Due to the large deformation of the inner steel after the steel comes into the plastic stage, the pressure between the inner steel tube and sandwiched concrete increases in the late phase of loading. For CFDST beam, presented in Fig. 14(b), the maximum contact stress occurs at the tensile side (point 4) between the outer steel tube and sandwiched concrete. This is because the concrete at point 4 undergoes the largest deformation in the section. Therefore, the outer steel tube exerts stronger contact stress to the sandwiched concrete.

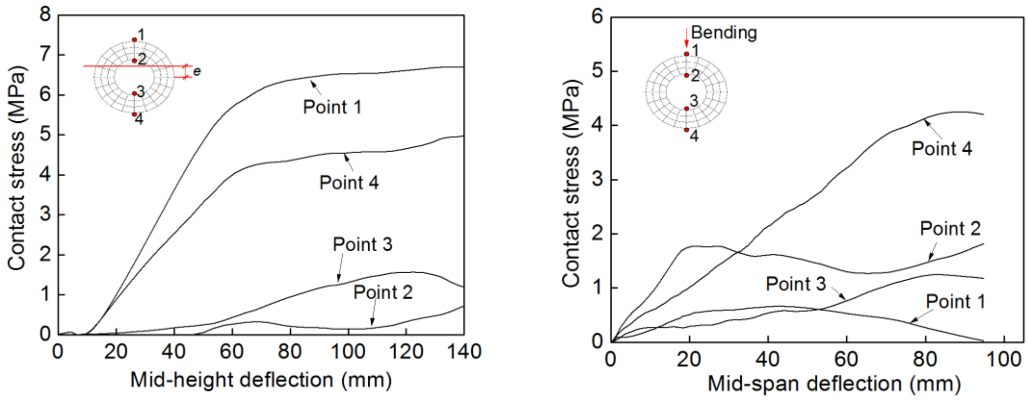

(a) Slender columns (b) Beams

Fig.14. Contact stress in the slender columns and beams.

4.2. Comparison with current design methods

Until now, there is no available design method for the CFDST slender columns and beams with stainless steel external tube. In 2018, Han et al. [3] proposed the design methods for estimating the load-bearing capacities of CFDST members with external carbon steel tube. Previous study conducted by Han et al. [19] showed that the formula to calculate the ultimate strength of the carbon steel CFDST stub column can be applied for such stub column with stainless steel external tube. Thus, in this section, this design rule suggested by Han et al. [3] is compared with the experimental and FE results to assess their applicability in CFDST slender columns and beams with external stainless jacket. In addition, the method for the carbon steel hollow CFST members in GB 50936 [26] is also modified by considering the contribution of the inner steel tube to predict the load-carrying capacities of CFDST members.

4.2.1 Design method by Han et al.

According to Han et al. [3], the buckling capacity N of the CFDST column is as follows:

$$N = \varphi N_{\mathrm{u}} \tag{4a}$$

where

$$\varphi = \begin{cases} 1 & \lambda \le \lambda_{\mathrm{o}} \\ a\cdot\lambda^2 + b\cdot\lambda + c & \lambda_{\mathrm{o}} < \lambda \le \lambda_{\mathrm{p}} \\ \dfrac{d\cdot(-0.23\chi^2+1)}{(\lambda+35)^2} & \lambda > \lambda_{\mathrm{p}} \end{cases} \tag{4b}$$

$$N_{\mathrm{u}} = f_{\mathrm{osc}}(A_{\mathrm{so}} + A_{\mathrm{c}}) + f_{\mathrm{yi}}A_{\mathrm{si}} \tag{4c}$$

$$f_{\mathrm{osc}} = \alpha/(1+\alpha)\cdot\chi^2\cdot f_{\mathrm{yo}} + (1+\alpha_{\mathrm{n}})/(1+\alpha)\cdot(1.14+1.02\xi)\cdot f_{\mathrm{c}} \tag{4d}$$

$$\xi=\frac{A_{\mathrm{so}}\cdot f_{\mathrm{yo}}}{A_{\mathrm{c,\,nominal}}\cdot f_{\mathrm{c}}}=\alpha_{\mathrm{n}}\cdot\frac{f_{\mathrm{yo}}}{f_{\mathrm{c}}} \tag{4e}$$

$$\alpha=A_{\mathrm{so}}/A_{\mathrm{c}} \tag{4f}$$

in which N_{u}= sectional capacity under compression, φ= buckling reduction coefficient, f_{osc}= compound compressive strength of the concrete and the outer steel tube, a, b, c and d are the parameters related to the buckling reduction coefficient, as presented detailly in Ref. [5].

The flexural capacity M_{u} of the CFDST member is expressed as:

$$M_{\mathrm{u}}=\gamma_{\mathrm{m1}}\cdot W_{\mathrm{scm}}\cdot f_{\mathrm{osc}}+\gamma_{\mathrm{m2}}\cdot W_{\mathrm{si}}\cdot f_{\mathrm{yi}} \tag{5a}$$

where

$$W_{\mathrm{scm}}=\frac{\pi\left(D_{\mathrm{o}}^{4}-D_{\mathrm{i}}^{4}\right)}{32D_{\mathrm{o}}} \tag{5b}$$

$$W_{\mathrm{si}}=\frac{\pi\left[D_{\mathrm{i}}^{4}-(D_{\mathrm{i}}-2t_{\mathrm{i}})^{4}\right]}{32D_{\mathrm{i}}} \tag{5c}$$

$$\gamma_{\mathrm{m1}}=0.48\ln(\xi+0.1)\cdot(1+0.06\chi-0.85\chi^{2})+1.1 \tag{5d}$$

$$\gamma_{\mathrm{m2}}=-0.02\chi^{-2.76}\ln\xi+1.04\chi^{-0.67} \tag{5e}$$

in which W_{scm}= compound section modulus of the concrete and the outer steel tube, W_{si}= section modulus of the internal steel tube.

The axial load N vs. bending moment M relationship of the CFDST member under combined compression and bending is presented in Eq. (6):

$$\begin{cases}\dfrac{N}{\varphi N_{\mathrm{u}}}+\dfrac{a_1}{d_1}\cdot\left(\dfrac{\beta_{\mathrm{m}}\cdot M}{M_{\mathrm{u}}}\right)=1 & \text{for } N/N_{\mathrm{u}}\geq 2\varphi^{3}\cdot\eta_{\mathrm{o}}\\ -b_1\cdot\left(\dfrac{N}{N_{\mathrm{u}}}\right)^{2}-c_1\cdot\left(\dfrac{N}{N_{\mathrm{u}}}\right)+\dfrac{1}{d_1}\cdot\left(\dfrac{\beta_{\mathrm{m}}\cdot M}{M_{\mathrm{u}}}\right)=1 & \text{for } N/N_{\mathrm{u}}<2\varphi^{3}\cdot\eta_{\mathrm{o}}\end{cases} \tag{6}$$

in which β_{m}= equivalent moment coefficient, as given in EC 4 (Table 6.4) [25], a_1, b_1, c_1 and d_1 are the parameters to control the N-M relation.

4.2.2 GB 50936

A unified equation is developed in Chinese code GB 50936 [26] for both solid and hollow CFST members, considering the influence of hollow ratio χ on the ultimate strengths. In this part, the cross-sectional compressive and flexural resistances in GB 50936 are modified by adding the contribution of the inner steel tube, as presented in Eqs. 7 and 8. The modified GB 50936 equations for the axial load-carrying capacity of slender column is expressed as:

$$N = \varphi\left[(A_{so}+A_c)f_{osc}+A_{si}f_{yi}\right] \tag{7a}$$

where

$$\varphi = \frac{1}{2\bar{\lambda}_{osc}^{\ 2}}\left[\bar{\lambda}_{osc}^{\ 2}+(1+0.25\bar{\lambda}_{osc}) - \sqrt{\left(\bar{\lambda}_{osc}^{\ 2}+\left(1+0.25\bar{\lambda}_{osc}\right)\right)^2 - 4\bar{\lambda}_{osc}^{\ 2}}\right] \tag{7b}$$

$$\bar{\lambda}_{osc} = (\lambda_{osc}/\pi)\sqrt{f_{osc}/E_{osc}} \tag{7c}$$

$$f_{osc}=(1.212+B\xi+C\xi^2)\cdot f_c \tag{7d}$$

$$E_{osc} = (E_{so}I_{so}+E_{si}I_{si}+E_cI_c)/I_{osc} \tag{7e}$$

$$\xi=\frac{A_{so}\cdot f_{yo}}{A_c\cdot f_c} = \alpha\cdot\frac{f_{yo}}{f_c} \tag{7f}$$

in which $\bar{\lambda}_{osc}$= non-dimensional slenderness; E_{osc}= Composite bending modulus.

The flexural capacity of the CFDST beam is given by

$$M_u=\gamma_m(W_{scm}\cdot f_{osc}+W_{si}\cdot f_{yi}) \tag{8a}$$

where

$$\gamma_m=(1-0.5\chi)(-0.483\xi+1.926\sqrt{\xi}) \tag{8b}$$

The load-carrying capacity of the CFDST beam-column is given as

$$\begin{cases} \dfrac{N}{\varphi N_u}+\dfrac{\beta_m\cdot M}{1.5M_u(1-0.4N/N_E)}=1 & \text{for } N/N_u\geq 0.255 \\ -\dfrac{N}{2.17N_u}-\dfrac{\beta_m\cdot M}{M_u(1-0.4N/N_E)}=1 & \text{for } N/N_u<0.255 \end{cases} \tag{9a}$$

where

$$N_E=\frac{\pi^2E_{osc}(A_{so}+A_{si}+A_c)}{\lambda_{osc}^2} \tag{9b}$$

The predicted ultimate compressive loads of slender columns and moment capacities of beams using Eqs. (4-9) are compared with the test and FE results in Fig. 15. The average ratio μ of the predicted results to experimental and FE results and corresponding standard deviation S are also given in Fig. 15. The comparison results demonstrate that generally, the design methods recommended by Han et al. [3] are acceptable for the design of the CFDST slender columns and beams having either external stainless or carbon steel tube. In general, the GB 50936 provides the conservative prediction for the ultimate strengths and bending capacities.

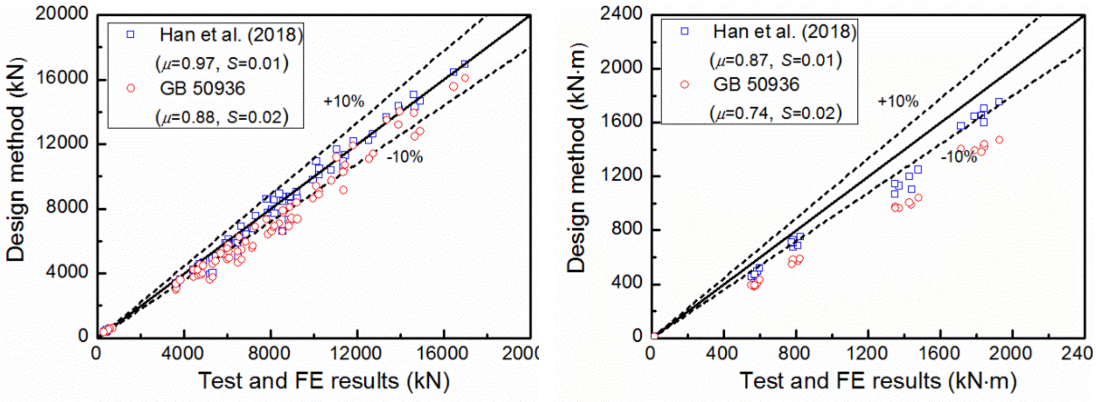

(a) Ultimate strengths of slender columns (b) Moment capacities of beams

Fig.15. Comparison between design method and test and FE results.

5. Conclusions

This work experimentally and numerically investigated the behaviours of CFDST slender columns and beams with stainless steel external tube. A total of 24 specimens were tested to obtain their failure patterns and load-deflection curves. The FE models were established to predict the experimental results and used to extend the parameter ranges. The obtained experimental and FE results were used to evaluate the acceptability of the design methods for CFDST members with carbon steel external tube proposed by Han et al. [3]. Within the parameter ranges of this work, the main conclusions are summarized as follows:

(1) The tested slender columns and beams presented ductile behaviour. The sandwiched concrete remained intact, which is mainly due to the confinement of the double-skin tubes. The failure patterns of CFDST members with external stainless steel tubes were similar to those of the CFST and CFDST members with outer carbon steel.

(2) The predicted load-bearing capacities and load-deflection developments of slender columns and beams using the finite element (FE) model present reasonable agreements with the experimental results. Through the parametric investigations, considering the structural efficiency, it is advised to adopt the high-strength outer steel tube and hollow ratio of 0.5 in CFDST member under combined compression and bending.

(3) The analysis of load distribution and confinement effect indicate that during the whole loading process, the external stainless steel tube, sandwiched concrete and inner carbon steel tube in the CFDST slender columns and beams could work together.

(4) The design methods for estimating the load-carrying capacities of CFDST slender columns and beams with external carbon steel tube proposed by Han et al. [3] yield acceptable predictions for such kind members with external stainless steel tube.

Acknowledgements

The research work was supported by the National Natural Science Foundation (No. 51838008).

References

[1] C.D. Goode, Y.T. Fatheldin, Sandwich cylinders (steel-concrete-steel) subjected to external pressure, ACI. J. 77 (2) (1980) 109-115.

[2] X.L. Zhao, L.H. Han, Double skin composite construction, Prog. Struct. Eng. Mater. 8 (3) (2006) 93-102.

[3] L.H. Han, D. Lam, D.A. Nethercot, Design guide for concrete-filled double skin steel tubular structures (1st Edition), CRC Press, UK, 2018.

[4] S. Wei, S.T. Mau, C. Vipulanandan, Performance of new sandwich tube under axial loading: experiment, J. Struct. Eng. 121 (12) (1995) 1806-14.

[5] Z. Tao, L.H. Han, X.L. Zhao, Behaviour of concrete-filled double skin (CHS inner and CHS outer) steel tubular stub columns and beam-columns, J. Constr. Steel Res. 60 (8) (2004) 1129-1158.

[6] K. Uenaka, H. Kitoh, K. Sonoda, Concrete filled double skin circular stub columns under compression, Thin-Walled Struct. 48 (2010) 19-24.

[7] Q.Q. Liang, Nonlinear analysis of circular double-skin concrete-filled steel tubular columns under axial compression, Eng. Struct. 131(2017) 639-650.

[8] Q.Q. Liang, Numerical simulation of high strength circular double-skin concrete-filled steel tubular slender columns, Eng. Struct. 168(2018) 205-217.

[9] W. Li, B. Chen, L.H. Han, D. Lam, Experimental study on the performance of steel-concrete interfaces in circular concrete-filled double skin steel tube, Thin-Walled Struct. 149 (2020) 106660.

[10] L.H. Han, H. Huang, Z. Tao, X.L. Zhao, Concrete-filled double skin steel tubular (CFDST) beam-columns subjected to cyclic bending, Eng. Struct. 28 (12) (2006) 1698-1714.

[11] R. Wang, L.H. Han, X.L. Zhao, K.J.R. Rasmussen, Experimental behavior of concrete filled double steel tubular (CFDST) members under low velocity drop weight impact, Thin-Walled Struct. 97 (2015) 279-295.

[12] W. Li, T. Wang, L.H. Han, Seismic performance of concrete-filled double-skin steel tubes after

exposure to fire: Experiments, J. Constr. Steel Res. 154 (2019) 209-223.

[13] H. Lu, L.H. Han, X.L. Zhao, Fire performance of self-consolidating concrete filled double skin steel tubular columns: Experiments, Fire. Saf. J. 45 (2) (2010) 106-115.

[14] W. Li, L.H. Han, X.L. Zhao, Axial strength of concrete-filled double skin steel tubular (CFDST) columns with preload on steel tubes, Thin-Walled Struct. 56 (2012) 9-20.

[15] F.C. Wang, Effective design of submarine pipe-in-pipe using Finite Element Analysis, Ocean Eng. 153 (2018) 23-32.

[16] N.R. Baddoo, Stainless steel in construction: A review of research, application, challenges and opportunities, J. Constr. Steel Res. 64 (11) (2008) 1199-1206.

[17] B. Uy, Z. Tao, L.H. Han, Behaviour of short and slender concrete-filled stainless steel tubular columns, J. Constr. Steel Res. 67 (2011) 360-378.

[18] L.H. Han, C.Y. Xu, Z. Tao, Performance of concrete filled stainless steel tubular (CFSST) columns and joints: Summary of recent research, J. Constr. Steel Res. 152 (2019) 117-131.

[19] L.H. Han, Q.X. Ren, W. Li, Tests on stub stainless steel-concrete-carbon steel double-skin tubular (DST) columns, J. Constr. Steel Res. 67(3) (2011) 437-452.

[20] M.F. Hassanein, Q.F. Kharoob, Q.Q. Liang, Circular concrete-filled double skin tubular short columns with external stainless steel tubes under axial compression, Thin-Walled Struct. 73 (2013) 252-263.

[21] F.C. Wang, L.H. Han, W. Li, Analysis behavior of CFDST stub columns with external stainless steel tubes under axial compression, Thin-Walled Struct. 127 (2018) 756-768.

[22] F.Y. Wang, B. Young, L. Gardner, Compressive testing and numerical modeling of concrete-filled double skin CHS with austenitic stainless steel outer tubes, Thin-Walled Struct. 141 (2019) 345-359.

[23] M.F. Hassanein, Q.F. Kharoob, Analysis of circular concrete-filled double skin tubular slender columns with external stainless steel tubes, Thin-Walled Struct. 79 (2014) 23-37.

[24] AISC. Load and resistance factor design specification, for structural steel buildings. American Institute of Steel Construction, Chicago, 2010.

[25] EN1994-1-1. Eurocode 4: Design of composite steel and concrete structures-Part 1-1: General

rules and rules for buildings. British Standard Institution, London, 2004.

[26] GB 50936-2014, Technical code for concrete filled steel tubular structures, Ministry of Housing and Urban-Rural Development of the People's Republic of China, 2014.

[27] ISO 6892-1, Metallic Materials Tensile Testing Part 1: Method of Test at Room Temperature, International Organization for Standardization, 2009.

[28] L.H. Han, H. Lu, G.H. Yao, F.Y. Liao, Further study on the flexural behaviour of concrete-filled steel tubes, J. Constr. Steel Res. 62 (2006) 554-565.

[29] L.H. Han, Concrete-filled steel tube structures: theory to practice (3rd Edition). Science Press, Beijing, 2016 (in Chinese).

[30] Q.X. Ren, L.H. Han, D. Lam, W. Li, Tests on elliptical concrete filled steel tubular (CFST) beams and columns, J. Constr. Steel Res. 99 (2014) 149-160.

[31] H. Yang, F.Q. Liu, T.M. Chan, W. Wang, Behaviour of concrete-filled cold-formed elliptical hollow section beam-columns with varying aspect ratios, Thin-Walled Struct. 120 (2017) 9-28.

[32] L.H. Han, Flexural behaviour of concrete-filled steel tubes, J. Constr. Steel Res. 60 (2004) 313-337.

[33] H. Yang, F.Q. Liu, L. Gardner, Post-fire behaviour of slender reinforced concrete columns confined by circular steel tubes, Thin-Walled Struct. 87 (2015) 12-29.

[34] L.H. Han, X.L. Zhao, Z. Tao, Tests and mechanics model for concrete-filled SHS stub columns, columns and beam-columns, Steel Compos. Struct. Int. J. 1(1) (2001) 51-74.

[35] K.J.R. Rasmussen, Full-range stress-strain curves for stainless steel alloys, J. Constr. Steel Res. 59 (1) (2003) 47-61.

[36] Z. Tao, B. Uy, F.Y. Liao, L.H. Han, Nonlinear analysis of concrete-filled square stainless steel tube columns under axial compression, J. Constr. Steel Res. 67 (11) (2011) 1719-1732.

[37] F.Q. Liu, Y.Y. Wang, T.M. Chan, Behaviour of concrete-filled cold-formed elliptical hollow sections with varying aspect ratios, Thin-Walled Struct. 110 (2017) 47-61.

[38] F.Q. Liu, H. Yang, R. Yan, W. Wei, Experimental and numerical study on behaviour of square steel tube confined reinforced concrete stub columns after fire exposure, Thin-Walled Struct. 139 (2019) 105-125.